Large-scale integration of MoS2 on high-TC superconducting YBa2Cu3O7 for the realization of Josephson devices

K. Seurre, M. Ayachi, F. Godel, S J Carreira, B. Dlubak, P. Seneor, V. Humbert, Javier Villegas

▶ **To cite this version:**

K. Seurre, M. Ayachi, F. Godel, S J Carreira, B. Dlubak, et al.. Large-scale integration of MoS2 on high-TC superconducting YBa2Cu3O7 for the realization of Josephson devices. Applied Physics Letters, 2024, 125 (9), pp.092603. 10.1063/5.0216735 . hal-04756959

HAL Id: hal-04756959
https://hal.science/hal-04756959v1

Submitted on 28 Oct 2024

HAL is a multi-disciplinary open access archive for the deposit and dissemination of scientific research documents, whether they are published or not. The documents may come from teaching and research institutions in France or abroad, or from public or private research centers.

L'archive ouverte pluridisciplinaire **HAL**, est destinée au dépôt et à la diffusion de documents scientifiques de niveau recherche, publiés ou non, émanant des établissements d'enseignement et de recherche français ou étrangers, des laboratoires publics ou privés.

AIP Publishing Applied Physics Letters ACCEPTED MANUSCRIPT

This is the author's peer reviewed, accepted manuscript. However, the online version of record will be different from this version once it has been copyedited and typeset.

PLEASE CITE THIS ARTICLE AS DOI: 10.1063/5.0216735

Large-scale integration of MoS_2 on high-T_C superconducting $YBa_2Cu_3O_7$ for the realization of Josephson devices

K. Seurre, M. Ayachi, F. Godel, S.J. Carreira, B. Dlubak, P. Seneor, V. Humbert, J.E. Villegas*

[1]Laboratoire Albert Fert, CNRS, Thales, Université Paris-Saclay, 91767 Palaiseau, France

High-T_C cuprate superconductors' growth conditions and their incompatibility with some of the most standard nanofabrication approaches make their large-scale integration with 2D materials (such as graphene, transition metal dichalcogenides, and other Van der Waals materials) much more difficult than for conventional, metallic superconductors. Here we address this challenge and develop an approach based on pulsed laser deposition that allows the growth of the 2D semiconductor MoS_2 on the archetypal high-T_C superconductor $YBa_2Cu_3O_{7-x}$ (YBCO). This yields functional heterostructures in which the individual constituents' properties are preserved and that show superconducting coupling across their interface. The developed approach paves the way for large-scale 2D semiconductor co-integration with high-T_C superconductors towards the study and leverage of the superconducting proximity effect in hybrid devices.

*javier.villegas@cnrs-thales.fr

AIP Publishing Applied Physics Letters ACCEPTED MANUSCRIPT
This is the author's peer reviewed, accepted manuscript. However, the online version of record will be different from this version once it has been copyedited and typeset.
PLEASE CITE THIS ARTICLE AS DOI: 10.1063/5.0216735

The pioneering exfoliation of graphene[1] and the subsequent unveiling of its outstanding electrical properties [2] rapidly highlighted opportunities for novel electronic[3] and spintronic[4] devices. Such interest has then quickly been extended to a broader family of 2D materials including, among others, transition metal dichalcogenides (TMDCs)[5], Xenes[6], or 2D oxides[7]. Thanks to their unique "surface-like" behavior, a widely explored strategy has consisted in fostering and exploiting proximity-coupling and interfacial effects by combining 2D materials with others in heterostructures, towards discovering new phenomena and applications. One of the prototypical examples is the combination of 2D materials with superconductors. The physics of these hybrid heterostructures attracts much interest for fundamental and technological reasons. This is well illustrated by the use of 2D materials as the weak link of Josephson junctions, where specificities such as the Dirac band structure result in novel physics[8] and functionalities: for example, gate-tunable Josephson effects[9] for reconfigurable superconducting electronics[10].

Most of the work in this field has been based on conventional (*s-wave*) low critical temperature (T_C) superconductors, combined e.g. with graphene[9,11], topological insulators (TIs)[12,13], and TMDCs like MoS_2[14–17]. However, extensions of those studies to unconventional (*d-wave*) high-T_C cuprate superconductors (HTS) have remained much scarcer, despite their fundamental appeal and technological potential [18–20]. Indeed, combining 2D materials with HTS in heterostructures is challenging from a materials science standpoint. On one hand, HTS require epitaxial growth on specific substrates, at high temperatures (hundreds of ºC), and in an oxygen-rich atmosphere. This has hampered the standard approach of direct growth onto materials such as graphene or TDCMs flakes conventionally used with low-Tc metallic superconductors [9,15–17,21]. On the other hand, the transfer of 2D materials onto HTS is also problematic because these complex oxides are relatively delicate materials: their oxygen stoichiometry (which controls their physical properties) is extremely sensitive to the after-growth handling conditions (temperature, oxygen partial pressure, humidity)[22]. All of that imposes strong constraints. While a few experiments have surmounted the challenge and fabricated proximity devices that combine HTS with graphene[23–25] or a few different topological insulators (TIs)[26], this was only achieved via transfer techniques and, overall, the accessible heterostructures and fabrication methods

AIP Publishing Applied Physics Letters ACCEPTED MANUSCRIPT
This is the author's peer reviewed, accepted manuscript. However, the online version of record will be different from this version once it has been copyedited and typeset.
PLEASE CITE THIS ARTICLE AS DOI: 10.1063/5.0216735

are relatively limited as compared to the case of conventional superconductors. This motivates the development of approaches for integrating HTS and 2D materials in heterostructures, preserving their individual physical properties and yielding interfaces of good quality. Ideally, such integration should be done over large scales, to facilitate its technological exploitation.

Here we show that such large-scale integration can be entirely realized without relying on transfer techniques, by using instead pulsed laser deposition (PLD). PLD is widely used for the growth of thin films of HTS such as $YBa_2Cu_3O_{7-x}$ (YBCO)[27,28] and many other correlated oxides. Recently, it has also been used to grow individual TMDCs monolayers[29,30]. We demonstrate here its potential for the growth of HTS/TMDC heterostructures using an archetypal combination: MoS_2 grown on YBCO. As shown below, a critical aspect of this integration is the preservation of YBCO stoichiometry during MoS_2 growth. This is illustrated by varying the MoS_2 growth conditions and monitoring how they affect the superconducting T_C of YBCO. Finally, the functional properties of the optimized HTS/TMDC stack are demonstrated –beyond the characterization of the individual layers– by achieving Josephson coupling across the MoS_2 in vertical heterostructures. The obtained results pave the way for exploring proximity and interfacial effects in a large library of HTS/TMDC heterostructures and lift a barrier towards their large-scale exploitation in superconducting devices and circuits.

In the first fabrication step, a c-axis YBCO (50 nm-thick) film is grown on (001) oriented $SrTiO_3$ (STO) covered with a 6 nm-thick (001) CeO_2 buffer layer. This is done using a PLD system with KrF excimer laser (λ =248 nm), with 94mJ pulses at a repetition rate of 2Hz. The stoichiometric YBCO target is pre-ablated before deposition, which takes place under an O_2 pressure of 0.36 mbar at T=670°C (temperature of the rotating sample holder). After growth, the oxygen pressure is raised to 700 mbar and kept at this level during cooldown, to obtain optimal oxygenation. Once at room temperature, a 10 nm-thick Au capping layer, which protects the YBCO surface, is deposited *in situ* and yields highly-transparent Au/YCBO interface, as well as improves the electrical contact with other materials deposited on top [25,26,33]. The growth of MoS_2 is carried out in a second step, using a PLD chamber equipped with a tripled frequency Nd:YAG (355nm) laser. Several growth conditions were tested to optimize MoS_2 growth while preserving the superconducting properties of YBCO. We varied the three parameters

AIP Publishing Applied Physics Letters ACCEPTED MANUSCRIPT
This is the author's peer reviewed, accepted manuscript. However, the online version of record will be different from this version once it has been copyedited and typeset.
PLEASE CITE THIS ARTICLE AS DOI: 10.1063/5.0216735

shown in **Figure 1a**: the growth temperature, the deposition time, and the presence of oxygen during the warm-up and cooldown ramps. Either a pure Ar (10^{-1} mbar) or O_2 (300 mbar) atmosphere was set during warm-up. Once the growth temperature T_{growth} is reached, the chamber atmosphere is set to Ar (10^{-1} mbar), and the deposition is carried out (stoichiometric MoS_2 target, 60mJ laser pulses at a repetition frequency of 2.5 Hz) for a time that determines the MoS_2 thickness. After deposition and before cooldown, the same atmosphere (Ar or O_2) as for warm-up is set in the chamber.

Figures 1b, c, and d show the normalized resistance *vs*. temperature for samples in which MoS_2 is grown under different conditions on the YBCO/STO substrate, to illustrate the impact on the superconducting properties of YBCO. The measurements were carried out using a 4-probe configuration by contacting the corners of the samples, the resistance was calculated as $R = \big(V(I) - V(-I)\big)/2I$, with $I = 10\mu A$ the injected current and V the measured voltage. **Figure 1b** illustrates the influence of the presence/absence of oxygen during the temperature ramps (T-ramps): the sample grown in the absence O_2 during the T-ramps shows depressed superconductivity, with a wide, incomplete transition towards zero-resistance whose onset is ~30 K lower than for the sample for which O_2 is present (here $T_c^{YBCO} \sim 75\ K$). This suggests that samples warmed/cooled in Ar are oxygen-depleted. **Figure 1c** shows resistance versus temperature characteristics R(T) for three samples in which MoS_2 has been grown with different $T_{growth} = 255$°C, 310°C, and 430°C but otherwise identical conditions (O_2 was applied during the T-ramps and the deposition time was 5 min). Here $T_{growth} = 255$°C corresponds to the lowest growth temperature compatible with good MoS_2 properties and 430°C corresponds to previously reported growth temperature ~400°C used for TMDCs[29,30]. One can see that when T_{growth} is increased the superconducting properties are rapidly suppressed. Already for $T_{growth} = 310$°C there is no trace left of the superconducting transition: the resistance shows a metallic behavior likely dominated by the Au layer. For $T_{growth} = 430$°C, the R(T) shows insulating behavior as expected for severely oxygen-depleted YBCO[31]. The fact that this is probed indicates that the Au layer is no longer shunting the electrical current, presumably because T_{growth} is high enough to promote Au atom diffusion and segregation, leading to a discontinuity of the Au layer. **Figure 1d** shows R(T) for three samples grown in identical conditions ($T_{growth} = 255$°C and O_2 during the T-ramps) but with different MoS_2 deposition

AIP Publishing Applied Physics Letters ACCEPTED MANUSCRIPT
This is the author's peer reviewed, accepted manuscript. However, the online version of record will be different from this version once it has been copyedited and typeset.
PLEASE CITE THIS ARTICLE AS DOI: 10.1063/5.0216735

times. All three show a superconducting transition. However, the T_C decreases with the deposition time suggesting a progressive de-oxygenation of YBCO when heated in pure Ar atmosphere during the MoS_2 growth, even for T_{growth} as low as 255°C. Unfortunately, it is not possible to maintain the O_2 during the growth because oxygen atoms partially replace sulfur, degrading the MoS_2 layer. Hence, to protect as much as possible the YBCO properties, the MoS_2 deposition must be restricted to short times, which as shown below is not a strong constraint if we aim to grow a very thin MoS_2 . Based on T_{growth} = 255 °C that allowed protecting at best the YBCO properties, we fabricated heterostructures with different MoS_2 thickness and characterized their structural properties. Fig. 2a shows a typical X-ray diffraction pattern that demonstrates textured YBCO growth along the (001) axis[32] . Because of their very close scattering vector and due to the peak broadening caused by the finite thickness, the (002) reflection of MoS_2 [33] appears convoluted with that of YBCO. This is evidenced by the doubling of this peak's width as compared the YBCO (001) one. The absence of other MoS_2 reflections confirms textured growth along its (001) crystallographic direction. Atomic Force Microscopy (see example in Fig. 2b) was carried out on two areas of the samples, the one being the bare YBCO/Au surface, the other being covered by MoS_2 (the areas were defined by locally etching MoS_2 via oxygen plasma). The root-mean-square surface roughness of MoS_2 σ_{MoS_2}~3.6 nm, is slightly higher than that of Au σ_{Au}~3 nm. Measurements of the steps height between both areas (see Fig. 2b) in a series of MoS_2 layers with different deposition times allowed us to estimate the growth rate 7.2±0.8 nm min^{-1}. To further ascertain the quality of the MoS_2, we used Raman spectroscopy[34]. Typical spectra for MoS_2 and Au surface areas are shown in **Figure 2c**, taken by using a 514 nm laser, a 3000l/mm grating, under 5mW illumination for 10s. The spectrum measured on the MoS_2 area (blue) shows two peaks at 383.5cm^{-1} and at 406cm^{-1} which are absent in the control area (red spectrum). Those peaks correspond to the characteristic E^1_{2g} and A_{1g} Raman shifts for MoS_2 [34]. To evaluate the sample homogeneity, we looked at the variations of the A_{1g}/E^1_{2g} ratio, plotted in **Figure 2b** as a function of the *x*-*y* coordinates over a 6 µm x 6 µm area. The ratio is nearly constant, with small variations around $A_{1g}/E^1_{2g} \sim 4.7$, which indicates the homogeneity of the MoS_2 layer over the probed length scale. All of the above confirms the good structural properties of the grown heterostructures.

AIP Publishing Applied Physics Letters ACCEPTED MANUSCRIPT
This is the author's peer reviewed, accepted manuscript. However, the online version of record will be different from this version once it has been copyedited and typeset.
PLEASE CITE THIS ARTICLE AS DOI: 10.1063/5.0216735

To demonstrate the functional properties of the YBCO/MoS_2 heterostructures, and to characterize the electrical properties of MoS_2, we fabricated YBCO/MoS_2/$Mo_{80}Si_{20}$ vertical Josephson junctions (as sketched in **Figure 3b**). Here $Mo_{80}Si_{20}$ (MoSi), which is an amorphous *s-wave* superconductor with $T_C^{MoSi} \sim 5\ K - 6\ K$ [30], is conveniently used as a top electrode because it can be easily implemented via a simple lithography approach, contrary to YBCO whose restrictive growth conditions make its growth on MoS_2 extremely challenging. In particular, we use UV photolithography (see details elsewhere[35,36]) to define micrometric square apertures in a resist layer deposited on top of the MoS_2. Subsequently, a 100 nm thick layer of MoSi capped with 50 nm of Au was deposited by sputtering. This way, MoSi contacts the MoS_2 surface only through the square aperture in the resist (indicated with an arrow in the microscopy image shown in **Fig. 3a**), yielding junctions with an area in the 10 μm x 10 μm range. Four-probe electrical measurements of the junctions were then carried out by directly wire-bonding the YBCO and the MoSi electrodes as sketched in **Fig. 3b**. Current-biased $V(I)$ and differential conductance dI/dV measurements were performed using the delta-mode of a Keithley 6221 current source coupled to a 2182 nanovoltmeter.

Figure 3c presents typical dI/dV *vs.* I for temperatures 2 K ≤ T ≤ 10K below the $T_C^{YBCO} \sim 85\ K$ for this device. The curves are essentially symmetric around zero bias. For $T = 10$ K > T_C^{MoSi}, we observe high conductance (~10^4 S) at low bias, followed by a gradual decrease (down to ~ 300 S) as the bias is increased. The behavior dramatically changes around $T = 5$ K ~ T_C^{MoSi}. Already at $T = 5$ K the low-bias conductance is significantly lower (~10^3 S) than above, resulting in a flatter curve. As the temperature is further decreased to $T = 4.9 - 4.7$ K, the low-bias conductance rapidly drops to the tens of S level. Indeed, within this temperature range the curve's shape is inverted: a "dip" appears within the low-bias range, followed by a sudden increase with increasing bias, ultimately leading to a similar conductance level as for higher temperatures. For $T \leq 4$ K, the low-conductance level extends over all the probed bias range, except around zero bias. Indeed, for $T <$ 4.7 K a zero-bias peak develops which becomes higher as the temperature becomes lower, especially below 3 K. This peak results from the transition to a zero-resistance state, as it can be deduced from the corresponding $V(I)$ shown in the main panel of **Fig. 3d**. One can see that, at the lowest temperatures and within a low-bias range, current

AIP Publishing Applied Physics Letters ACCEPTED MANUSCRIPT
This is the author's peer reviewed, accepted manuscript. However, the online version of record will be different from this version once it has been copyedited and typeset.
PLEASE CITE THIS ARTICLE AS DOI: 10.1063/5.0216735

injection leads to zero voltage drop. This allows defining a superconducting critical current $I_C \approx 200$ μA for the measurement at 2 K. I_C quickly vanishes as the temperature is increased, as finely evidenced by the gradual disappearance of the zero-bias conductance peak in the differential conductance, see **Figure 3c**. The $V(I)$ for another junction is shown in the inset of **Fig. 3d** and displays a similar behavior with $I_C \approx 110$ μA at T=2 K.

The inset of **Fig. 3c** shows direct conductance I/V measured at high I=40 mA and low T=2 K for ~20 different junctions with either 0, ~5.6 nm or ~15.5 nm thick MoS_2. This conductance corresponds high-current limit "plateau" observed in the main panel of **Fig. 3c**. One can see that the conductance decreases exponentially as the MoS_2 thickness increases, as expected for MoS_2 behaving as a tunneling barrier.

The temperature-dependent conductance features described above can be explained as follows. For $T_C^{MoSi} < T = 10\ K < T_C^{YBCO}$, the bias dependence is the one typically observed in finite-transparency junctions between a normal metal and a *d-wave* superconductor, which typically display a high conductance at low bias followed by a strong decrease with increasing bias[37,38]. This behavior may result from two mechanisms: the first one is tunneling into characteristic zero-energy quasiparticle-bound states at the surface of the *d-wave* superconductor[39]. The second is the current-driven depression of superconductivity near the interface. Both mechanisms can be concomitant.

The radically different behavior for $T < 5$ K is associated with the onset of superconductivity in MoSi. The strong conductance drop within the low-bias range is as expected from the energy gap opening in a conventional (*s-wave*) superconductor, which leads to a vanishing density of electronic states around the Fermi level. Here, thermally excited Bogoliubov quasiparticles are the only available states, whose population diminishes as the temperature is lowered, largely hindering single-particle tunneling into the superconductor[40]. That explains the strong conductance drop over a bias range that gradually extends as the temperature is decreased (Fig. 3d). The quasiparticle current across the junction is thus strongly suppressed as MoSi turns superconducting. This, together with the behavior observed in the inset of Fig. 3c, rules out the junctions' conductance is dominated by pinholes and supports that

AIP Publishing Applied Physics Letters ACCEPTED MANUSCRIPT
This is the author's peer reviewed, accepted manuscript. However, the online version of record will be different from this version once it has been copyedited and typeset.
PLEASE CITE THIS ARTICLE AS DOI: 10.1063/5.0216735

MoS_2 behaves as a tunneling barrier. While quasiparticle tunneling is limited upon opening of the superconducting gap in MoSi, Cooper pairs can flow across the device as long as the current is kept below a certain critical I_C (**Fig. 3d**), yielding the emergent zero-bias conductance peak.

A quantitative analysis of the transport measurements would likely require adapting existing models. e.g. for tunneling [39] and Josephson effects [41] in d-wave superconductor junctions, to our junctions' specificities. While this is beyond the scope of the word, from the above observations, a picture emerges. It is clear from the inset of **Fig. 3c** that, in the presence of a MoS_2 layer, the junctions' conductance is not dominated by the YBCO/Au interface, but instead by the MoSi/MoS_2 one and MoS_2 layer, which behave as a tunneling barrier. Indeed, when MoSi is in its normal state, the bias-dependent conductance reflects characteristics of electron tunneling from this electrode into the "*d-wave* stack". The latter includes YBCO, the thin Au capping (which must be fully proximitized considering its thickness and the transparent interface expected from in-situ deposition[23,24,42]), and maybe part of the MoS_2 layer which, based on experiments on this material in contact with metallic superconductors[15], could be at least partially proximitized. As MoSi enters its superconducting state, the opening of the energy gap hinders single-particle injection, yielding the conductance drop for finite bias. However, at sufficiently low temperatures, Josephson coupling between the "*d-wave* stack" and MoSi is achieved, and a supercurrent (Cooper pair) flow is observed.

In summary, we have presented here the conditions for the PLD growth and integration of the 2D semiconductor MoS_2 with the high-T_C oxide superconductor YBCO in functional heterostructures. To illustrate the developed approach's potential, we have fabricated superconducting junctions that display Josephson coupling between YBCO and a conventional superconductor (MoSi) across MoS_2. This realization paves the way to exploring proximity behavior between HTS and TMDCs in its many facets (doping dependence, length scales, …) via 2D material gating, a property unavailable yet, as well as leveraging them for applications. Because the growth of high-T_C oxides on TMDCs appears an extremely challenging endeavor given their very restrictive growth conditions, the realization of those prospects will likely require implementing the PLD approach to fabricate planar proximity devices with the superconductor at the bottom[23,24,42]. That constitutes the next step towards gate-tunable high-T_C

AIP Publishing Applied Physics Letters ACCEPTED MANUSCRIPT
This is the author's peer reviewed, accepted manuscript. However, the online version of record will be different from this version once it has been copyedited and typeset.
PLEASE CITE THIS ARTICLE AS DOI: 10.1063/5.0216735

superconducting large-scale devices (superconducting quantum interferometers, SQIFs and similar arrays used in applications[43]) based on TMDCs and HTS.

Acknowledgments

We acknowledge funding from French ANR through grants ANR-22-CE24-0009-01 "SEEDS", ANR-22-CE30-00020-01 "SUPERFAST", ANR-22-EXSP-0007 PEPR SPIN "SPINMAT" and ANR-22-PEEL-0011 PEPR ELEC "ADICT", the European Union's Horizon 2020 research and innovation program under the Marie Sklodowska-Curie grant agreement 101029978 and EIC pathfinder grant 101130224 "JOSEPHINE", as well as the COST action "SUPERQUMAP".

AIP Publishing Applied Physics Letters ACCEPTED MANUSCRIPT
This is the author's peer reviewed, accepted manuscript. However, the online version of record will be different from this version once it has been copyedited and typeset.
PLEASE CITE THIS ARTICLE AS DOI: 10.1063/5.0216735

References

[1] K.S. Novoselov, A.K. Geim, S. V Morozov, D. Jiang, Y. Zhang, S. V Dubonos, I. V Grigorieva, and A.A. Firsov, "Electric field effect in atomically thin carbon films," Science (1979) **306**(5696), 666–669 (2004).

[2] S. Das Sarma, S. Adam, E.H. Hwang, and E. Rossi, "Electronic transport in two-dimensional graphene," Rev Mod Phys **83**(2), 407 (2011).

[3] R. Wang, X.-G. Ren, Z. Yan, L.-J. Jiang, W.E.I. Sha, and G.-C. Shan, "Graphene based functional devices: A short review," Front Phys (Beijing) **14**, 1–20 (2019).

[4] P. Seneor, B. Dlubak, M.-B. Martin, A. Anane, H. Jaffres, and A. Fert, "Spintronics with graphene," MRS Bull **37**(12), 1245–1254 (2012).

[5] S. Manzeli, D. Ovchinnikov, D. Pasquier, O. V Yazyev, and A. Kis, "2D transition metal dichalcogenides," Nat Rev Mater **2**(8), 1–15 (2017).

[6] T. Wang, H. Wang, Z. Kou, W. Liang, X. Luo, F. Verpoort, Y. Zeng, and H. Zhang, "Xenes as an emerging 2D monoelemental family: fundamental electrochemistry and energy applications," Adv Funct Mater **30**(36), 2002885 (2020).

[7] P. Kumbhakar, C.C. Gowda, P.L. Mahapatra, M. Mukherjee, K.D. Malviya, M. Chaker, A. Chandra, B. Lahiri, P.M. Ajayan, and D. Jariwala, "Emerging 2D metal oxides and their applications," Materials Today **45**, 142–168 (2021).

[8] C.W.J. Beenakker, "Specular Andreev reflection in graphene," Phys Rev Lett **97**(6), 67007 (2006).

[9] H.B. Heersche, P. Jarillo-Herrero, J.B. Oostinga, L.M.K. Vandersypen, and A.F. Morpurgo, "Bipolar supercurrent in graphene," Nature **446**(7131), 56–59 (2007).

[10] C. Girit, V. Bouchiat, O. Naaman, Y. Zhang, M.F. Crommie, A. Zettl, and I. Siddiqi, "Tunable graphene dc superconducting quantum interference device," Nano Lett **9**(1), 198–199 (2009).

[11] X. Du, I. Skachko, and E.Y. Andrei, "Josephson current and multiple Andreev reflections in graphene SNS junctions," Phys Rev B **77**(18), 184507 (2008).

[12] M. Veldhorst, M. Snelder, M. Hoek, T. Gang, V.K. Guduru, X.L. Wang, U. Zeitler, W.G. van der Wiel, A.A. Golubov, and H. Hilgenkamp, "Josephson supercurrent through a topological insulator surface state," Nat Mater **11**(5), 417–421 (2012).

[13] C. Kurter, A.D.K. Finck, Y.S. Hor, and D.J. Van Harlingen, "Evidence for an anomalous current–phase relation in topological insulator Josephson junctions," Nat Commun **6**(1), 7130 (2015).

[14] M. Khezerlou, and H. Goudarzi, "Transport properties of spin-triplet superconducting monolayer MoS 2," Phys Rev B **93**(11), 115406 (2016).

[15] J.O. Island, G.A. Steele, H.S.J. Van Der Zant, and A. Castellanos-Gomez, "Thickness dependent interlayer transport in vertical MoS2 Josephson junctions," 2d Mater **3**(3), 31002 (2016).

[16] M. Ramezani, I.C. Sampaio, K. Watanabe, T. Taniguchi, C. Schonenberger, and A. Baumgartner, "Superconducting contacts to a monolayer semiconductor," Nano Lett **21**(13), 5614–5619 (2021).

AIP Publishing Applied Physics Letters ACCEPTED MANUSCRIPT
This is the author's peer reviewed, accepted manuscript. However, the online version of record will be different from this version once it has been copyedited and typeset.
PLEASE CITE THIS ARTICLE AS DOI: 10.1063/5.0216735

[17] A. Seredinski, E.G. Arnault, V.Z. Costa, L. Zhao, T.F.Q. Larson, K. Watanabe, T. Taniguchi, F. Amet, A.K.M. Newaz, and G. Finkelstein, "One-dimensional edge contact to encapsulated MoS2 with a superconductor," AIP Adv **11**(4), (2021).

[18] J. Linder, and A. Sudbø, "Tunneling conductance in s-and d-wave superconductor-graphene junctions: Extended Blonder-Tinkham-Klapwijk formalism," Phys Rev B **77**(6), 64507 (2008).

[19] D. Perconte, D. Bercioux, B. Dlubak, P. Seneor, F.S. Bergeret, and J.E. Villegas, "Superconducting Proximity Effect in d-Wave Cuprate/Graphene Heterostructures," Ann Phys **534**(8), 2100559 (2022).

[20] A. Di Bernardo, O. Millo, M. Barbone, H. Alpern, Y. Kalcheim, U. Sassi, A.K. Ott, D. De Fazio, D. Yoon, and M. Amado, "p-wave triggered superconductivity in single-layer graphene on an electron-doped oxide superconductor," Nat Commun **8**(1), 14024 (2017).

[21] T. Li, J. Gallop, L. Hao, and E. Romans, "Ballistic Josephson junctions based on CVD graphene," Supercond Sci Technol **31**(4), 045004 (2018).

[22] T. Ito, K. Takenaka, and S. Uchida, "Systematic deviation from T-linear behavior in the in-plane resistivity of YBa2Cu3O7-y: Evidence for dominant spin scattering," Phys Rev Lett **70**(25), 3995–3998 (1993).

[23] D. Perconte, F.A. Cuellar, C. Moreau-Luchaire, M. Piquemal-Banci, R. Galceran, P.R. Kidambi, M.B. Martin, S. Hofmann, R. Bernard, B. Dlubak, P. Seneor, and J.E. Villegas, "Tunable Klein-like tunnelling of high-temperature superconducting pairs into graphene," Nat Phys **14**(1), 25–29 (2018).

[24] D. Perconte, K. Seurre, V. Humbert, C. Ulysse, A. Sander, J. Trastoy, V. Zatko, F. Godel, P.R. Kidambi, S. Hofmann, X.P. Zhang, D. Bercioux, F.S. Bergeret, B. Dlubak, P. Seneor, and J.E. Villegas, "Long-Range Propagation and Interference of d -wave Superconducting Pairs in Graphene," Phys Rev Lett **125**(8), 87002 (2020).

[25] S. Jois, J.L. Lado, G. Gu, Q. Li, and J.U. Lee, "Andreev reflection and Klein tunneling in high-temperature superconductor-graphene junctions," Phys Rev Lett **130**(15), 156201 (2023).

[26] E. Wang, H. Ding, A. V Fedorov, W. Yao, Z. Li, Y.-F. Lv, K. Zhao, L.-G. Zhang, Z. Xu, and J. Schneeloch, "Fully gapped topological surface states in Bi2Se3 films induced by ad-wave high-temperature superconductor," Nat Phys **9**(10), 621–625 (2013).

[27] J.A. Greer, "High quality YBCO films grown over large areas by pulsed laser deposition," Journal of Vacuum Science & Technology A: Vacuum, Surfaces, and Films **10**(4), (1992).

[28] D.Q. Shi, R.K. Ko, K.J. Song, J.K. Chung, S.J. Choi, Y.M. Park, K.C. Shin, S.I. Yoo, and C. Park, "Effects of deposition rate and thickness on the properties of YBCO films deposited by pulsed laser deposition," Supercond Sci Technol **17**(2), (2004).

[29] F. Godel, V. Zatko, C. Carrétéro, A. Sander, M. Galbiati, A. Vecchiola, P. Brus, O. Bezencenet, B. Servet, M.B. Martin, B. Dlubak, and P. Seneor, "WS22D Semiconductor down to Monolayers by Pulsed-Laser Deposition for Large-Scale Integration in Electronics and Spintronics Circuits," ACS Appl Nano Mater **3**(8), (2020).

[30] V. Zatko, S.M.-M. Dubois, F. Godel, C. Carrétéro, A. Sander, S. Collin, M. Galbiati, J. Peiro, F. Panciera, and G. Patriarche, "Band-Gap Landscape Engineering in Large-Scale 2D Semiconductor van der Waals Heterostructures," ACS Nano **15**(4), 7279–7289 (2021).

AIP Publishing Applied Physics Letters ACCEPTED MANUSCRIPT
This is the author's peer reviewed, accepted manuscript. However, the online version of record will be different from this version once it has been copyedited and typeset.
PLEASE CITE THIS ARTICLE AS DOI: 10.1063/5.0216735

[31] J.P. Sydow, "Effects of oxygen content on ybco josephson junction structures," IEEE Transactions on Applied Superconductivity **9**(2 PART 3), (1999).

[32] R. El Hage, D. Sánchez-Manzano, V. Humbert, S. Carreira, V. Rouco, A. Sander, F. Cuellar, K. Seurre, A. Lagarrigue, S. Mesoraca, J. Briatico, J. Trastoy, J. Santamaría, and J.E. Villegas, "Disentangling Photodoping, Photoconductivity, and Photosuperconductivity in the Cuprates," Phys Rev Lett **132**(6), 066001 (2024).

[33] P. Joensen, R.F. Frindt, and S.R. Morrison, "Single-layer mos2," Mater Res Bull **21**(4), 457–461 (1986).

[34] C. Lee, H. Yan, L.E. Brus, T.F. Heinz, J. Hone, and S. Ryu, "Anomalous lattice vibrations of single- and few-layer MoS2," ACS Nano **4**(5), 2695–2700 (2010).

[35] V. Rouco, R. El Hage, A. Sander, J. Grandal, K. Seurre, X. Palermo, J. Briatico, S. Collin, J. Trastoy, K. Bouzehouane, A.I. Buzdin, G. Singh, N. Bergeal, C. Feuillet-Palma, J. Lesueur, C. Leon, M. Varela, J. Santamaría, and J.E. Villegas, "Quasiparticle tunnel electroresistance in superconducting junctions," Nat Commun **11**(1), 1–9 (2020).

[36] R. El Hage, V. Humbert, V. Rouco, G. Sánchez-Santolino, A. Lagarrigue, K. Seurre, S.J. Carreira, A. Sander, J. Charliac, S. Mesoraca, J. Trastoy, J. Briatico, J. Santamaría, and J.E. Villegas, "Bimodal ionic photomemristor based on a high-temperature oxide superconductor/semiconductor junction," Nat Commun **14**(1), (2023).

[37] C. Visani, Z. Sefrioui, J. Tornos, C. Leon, J. Briatico, M. Bibes, A. Barthélémy, J. Santamaria, and J.E. Villegas, "Equal-spin Andreev reflection and long-range coherent transport in high-temperature superconductor/half-metallic ferromagnet junctions," Nat Phys **8**(7), 539–543 (2012).

[38] G. Deutscher, "Andreev–Saint-James reflections: A probe of cuprate superconductors," Rev Mod Phys **77**(1), 109–135 (2005).

[39] S. Kashiwaya, and Y. Tanaka, "Theory for tunneling spectroscopy of anisotropic superconductors," Phys Rev B Condens Matter Mater Phys **53**(5), (1996).

[40] G.E. Blonder, M. Tinkham, and T.M. Klapwijk, "Transition from metallic to tunneling regimes in superconducting microconstrictions: Excess current, charge imbalance, and supercurrent conversion," Phys Rev B **25**(7), (1982).

[41] M.Y. Kupriyanov, and K.K. Likharev, "Josephson effect in high-temperature superconductors and in structures based on them," Soviet Physics Uspekhi **33**(5), 340 (1990).

[42] R. Baghdadi, S. Abay, D. Golubev, T. Bauch, and F. Lombardi, "Josephson effect through YBa2Cu3 O7-δ /Au-encapsulated nanogaps," Phys Rev B **95**(17), 174510 (2017).

[43] D. Crété, Y. Lemaître, B. Marcilhac, E. Recoba-Pawlowski, J. Trastoy, and C. Ulysse, "Optimal SQUID loop size in arrays of HTS SQUIDs," in *J Phys Conf Ser*, (IOP Publishing, 2020), p. 012012.

AIP Publishing Applied Physics Letters ACCEPTED MANUSCRIPT

This is the author's peer reviewed, accepted manuscript. However, the online version of record will be different from this version once it has been copyedited and typeset.

PLEASE CITE THIS ARTICLE AS DOI: 10.1063/5.0216735

AIP Publishing Applied Physics Letters ACCEPTED MANUSCRIPT
This is the author's peer reviewed, accepted manuscript. However, the online version of record will be different from this version once it has been copyedited and typeset.
PLEASE CITE THIS ARTICLE AS DOI: 10.1063/5.0216735

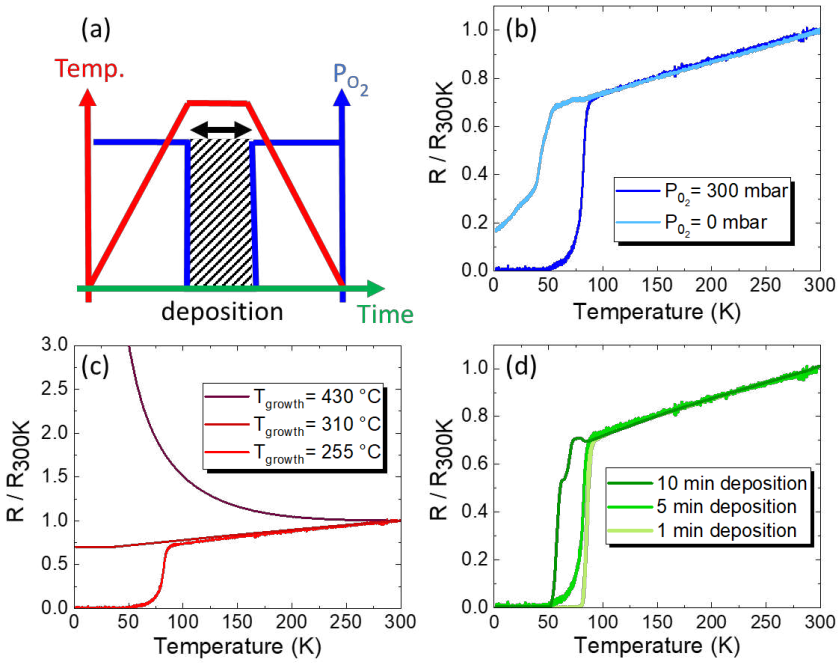

Figure 1 (a) Schematic representation of the parameters (temperature during deposition T_{growth}, oxygen pressure P_{O_2} during temperature ramps, and deposition time) used to control the growth of MoS_2 on the Au/YBCO//STO heterostructure. (b)-(d) Comparison of $R(T)$ characteristics for samples grown under varying conditions of (b) P_{O_2}, (c) temperature during deposition T_{growth} (d) deposition time; as indicated in the legends. $R(T)$ measurements are normalized to the resistance at T=300 K.

AIP Publishing Applied Physics Letters ACCEPTED MANUSCRIPT
This is the author's peer reviewed, accepted manuscript. However, the online version of record will be different from this version once it has been copyedited and typeset.
PLEASE CITE THIS ARTICLE AS DOI: 10.1063/5.0216735

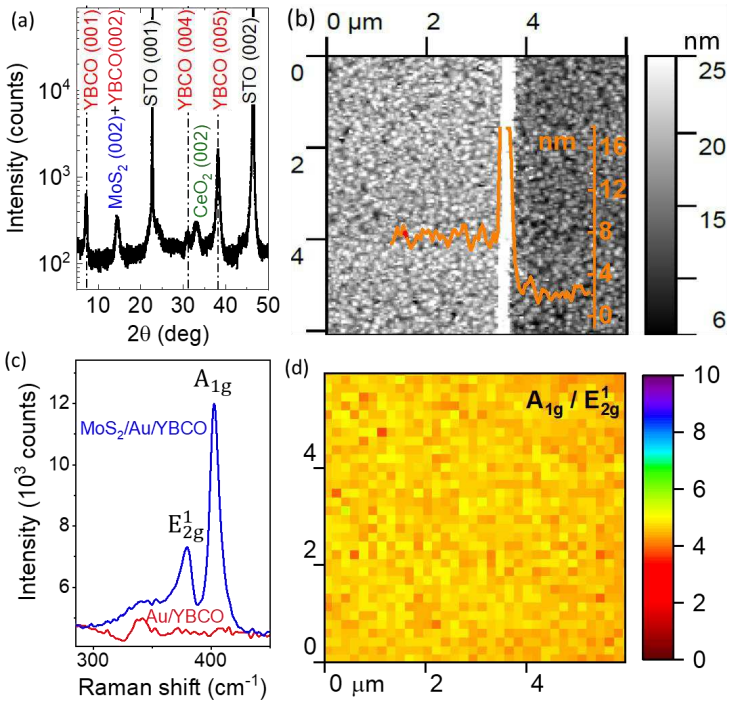

Figure 2 (a) X-ray diffraction spectrum (taken with λ_{Cu}=1.5418 Å) of a MoS_2 (20 nm)/Au (10 nm)/YBCO (50 nm) heterostructure on a CeO_2/STO substrate. The legends identify the reflection peaks. (b) Atomic force microscopy of a MoS_2 (5.4 nm)/Au (10 nm)/YBCO (50 nm) sample .On the right part of the image (darker area) the MoS_2 has been etched, exposing the Au surface. The inset shows a typical topography profile (line scan) across the boundary between both areas, the different heights at left and right sides being equal to the thickness of MoS_2. The white stripe corresponds to a ridge formed by the lithography and etching process (c) Raman spectra taken over Au/YBCO//STO (red) and MoS_2/Au/YBCO//STO (blue) from 280 to 460cm^{-1}. The characteristic A_{1g} and E^1_{2g} peaks of MoS_2 are identified. (b) 2D map depicting the ratio between the A_{1g} and E^1_{2g} peaks amplitude over a 6 µm x 6 µm area.

AIP Publishing Applied Physics Letters ACCEPTED MANUSCRIPT
This is the author's peer reviewed, accepted manuscript. However, the online version of record will be different from this version once it has been copyedited and typeset.
PLEASE CITE THIS ARTICLE AS DOI: 10.1063/5.0216735

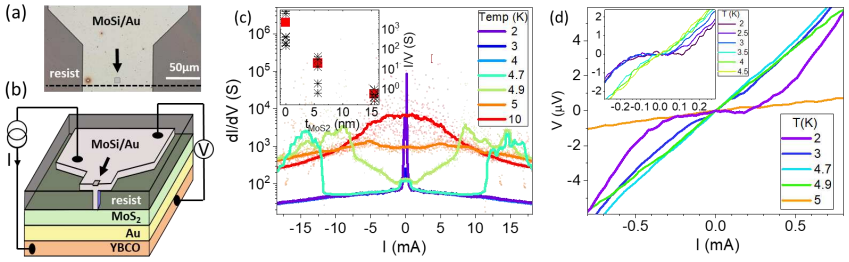

Figure 3 (a) Optical microscope image (top view) and (b) cross-section scheme of one of the studied Josephson junctions. The conductance of the device is measured by injecting current I and measuring voltage V in a four-point configuration as illustrated. (c) differential conductance of a 10 μm x 10 μm MoSi(100nm)/MoS_2(5.6nm)/Au(10nm)/YBCO(50nm) junction at various temperatures ranging from 10 to 2K. The inset shows the conductance at I=40 mA at T=2 K for a series of junctions with different MoS_2 thickness t_{MoS2} . Black crosses are the values for individual junctions (around 6 per each t_{MoS2}) and red dots are their average. (d) $V(I)$ characteristic of heterojunction. The inset of (d) shows the $V(I)$ characteristics of a smaller junction (7.5 μm x 7.5 μm).